Direct Growth of Highly Organized Crystalline Carbon Nitride from Liquid-Phase Pulsed Laser Ablation

Li Yang,*,† Paul W. May,† Lei Yin,‡ Richard Brown,† and Tom B. Scott§

School of Chemistry, University of Bristol, Cantock's Close, Bristol BS8 1TS, United Kingdom, Department of Aerospace Engineering, University of Bristol, Queen's Building, University Walk, Bristol BS8 1TR, United Kingdom, and Interface Analysis Centre, University of Bristol, Oldbury House, 121 St. Michael's Hill, Bristol BS2 8BS, United Kingdom

Received June 27, 2006. Revised Manuscript Received August 7, 2006

The novel technique of liquid-phase pulsed laser ablation has been used to obtain unique, highly ordered nanostructures of crystalline carbon nitride (C_3N_4) via ablation of a graphite target submerged in aqueous ammonia solution. Transmission electron microscopy (TEM) analysis shows that the morphology of the carbon nitride material changes at different length scales, depending upon the synthesis conditions. The initial ablation product comprises spherical nanoparticles of carbon nitride, which then elongate to nanorods (10 nm by ∼200 nm) with further ablation. Given sufficient concentration, the nanorods aggregate to form multilayered structures, and then ultimately larger, ordered "leaf-shaped" structures 30−50 nm by ∼200 nm in size. With even higher concentration, these leaflike structures can themselves aggregate to create interconnected networks of large micrometer scale clusters, which ultimately rearrange to micrometer-sized flowerlike structures. The various nanostructures were characterized using a number of analysis techniques, and their composition was found to be consistent with that of crystalline α- or β-phase carbon nitride. A formation mechanism for these structures is proposed that rationalizes the observed morphologies.

Introduction

There have been many ongoing attempts to produce covalently bonded compounds from the low-mass atomic elements, such as carbon and other neighboring elements in the periodic table.[1−6] Most of this research is motivated by the extraordinary combination of physical properties possessed by the binary compounds that have been synthesized to date. For example, boron carbide (B_4C) is an extremely hard material used in aircraft gyroscopes, silicon carbide (SiC) is a wide band gap semiconductor with uses in power electronics, and silicon nitride (Si_3N_4) is used as a passivation and etch resistant layer in integrated circuit fabrication.

One related compound, carbon nitride, C_3N_4, has received particular attention recently because of the prediction [7,8] that it should possess a hardness comparable to that of diamond, combined with high toughness and excellent tribological, electronic, and chemical properties. These properties may allow it to be used in applications such as electron emission devices, variable band gap semiconductors, and transparent hard coatings.[9] According to theoretical predictions,[7,8] C_3N_4 can adopt several different crystalline structures, including α-C_3N_4, β-C_3N_4, graphitic-C_3N_4 (g-C_3N_4), pseudocubic-C_3N_4, and cubic-C_3N_4. Among these forms, α-C_3N_4 and g-C_3N_4 are predicted to be the most energetically stable phases, then β-C_3N_4, with cubic- and pseudocubic-C_3N_4 being significantly higher in energy. The β-C_3N_4 structure is based on the β-Si_3N_4 structure, with carbon being four-coordinated with nitrogen and nitrogen three-coordinated with carbon.[6] α-C_3N_4 can be described as an ABAB stacking sequence of layers of β-C_3N_4 (A) and its mirror image (B). Because α-C_3N_4 and β-C_3N_4 have similar total energies, crystal structures, compositions, bulk moduli, band gaps, and atomic densities, it is very difficult to synthesize a single phase of only α-C_3N_4 or β-C_3N_4.

Disappointingly, synthesis of crystalline carbon nitride has proven to be far from straightforward. To date, a variety of deposition methods, such as radio frequency plasma deposition,[10] pulsed laser ablation in a vacuum,[11] ion-beam-assisted deposition,[12] ion implantation,[13] and magnetron sputtering,[14] have yielded mainly amorphous CN_x films, although there

* To whom correspondence should be addressed. E-mail: li.yang@bris.ac.uk.
† School of Chemistry, University of Bristol.
‡ Department of Aerospace Engineering, University of Bristol.
§ Interface Analysis Centre, University of Bristol.

(1) Zhao, H. Z.; Chen, X. L.; Jia, C. C.; Zhou, T.; Qu, X. H.; Jian, J. K.; Xu, Y. P.; Zhou, T. *Mater. Sci. Eng., B* **2005**, *122*, 226.
(2) Kundoo, S.; Banerjee, A. N.; Saha, P.; Chattopadhyay, K. K. *Mater. Lett.* **2003**, *57*, 2193.
(3) Fuge, G. M.; Rennick, C. J.; Pearce, S. R. J.; Henley, S. J.; May, P. W.; Ashfold, M. N. R. *Diamond Relat. Mater.* **2003**, *12*, 1049.
(4) Cao, Y.; Chen, X.; Lan, Y.; Li, J.; Xu, Y.; Xu, T. *Appl. Phys. A* **2000**, *71*, 465.
(5) Kawaguchi, M.; Yagi, S.; Enomoto, H. *Carbon* **2004**, *42*, 345.
(6) Liu, A. Y.; Cohen, M. L. *Science* **1989**, *245*, 841.
(7) Liu, A. Y.; Wentzcovitch, R. M. *Phys. Rev. B* **1994**, *50*, 10362.
(8) Teter, D. M.; Hemley, R. J. *Science* **1996**, *271*, 53.
(9) Wei, J.; Hing, P.; Mo, Z. Q. *Surf. Interface Anal.* **1999**, *28*, 208.
(10) Kumar, S.; Butcher, K. S. A.; Tansley, T. L. *J. Vac. Sci. Technol., A* **1996**, *14*, 2687.
(11) Bousetta, A.; Lu, M.; Bensaoula A.; Shultz, A. *Appl. Phys. Lett.* **1994**, *65*, 696.
(12) Hammer, P.; Victoria, N. M.; Alvarez, F. *J. Vac. Sci. Technol., A* **2000**, *18*, 2277.
(13) Niu, C. M.; Lu, Y. Z.; Lieber, C. M. *Science* **1993**, *261*, 334.
(14) Lopez, S.; Dunlop, H. M.; Benmalek, M.; Tourillon, G.; Wong, M.-S.; Sproul,W. D. *Surf. Interface Anal.* **1998**, *25*, 315.

10.1021/cm061485e CCC: $33.50
Published on Web 09/20/2006

are some reports of submicrometer quantities of crystalline material contained within the films.[3−5,15−16] However, to verify experimentally the theoretical predictions regarding the properties of C_3N_4, we need to perform measurements on larger, isolated crystals or on bulk microcrystalline films. A step toward this goal was recently reported by Yin and coworkers,[17] who reported the synthesis of highly crystalline β-carbon nitride nanorods using a combination of mechanically ground graphite nanoparticles and high-temperature chemical reaction.

We now report the successful nanoscale growth of crystalline carbon nitride using the novel method of liquid-phase pulsed laser ablation (LP-PLA). This technique involves focusing a high-power laser beam onto the surface of a solid target (in our case, graphite), which is submerged beneath a liquid. The interaction of the laser with the target causes the surface to vaporize in the form of an ablation plume, which contains species such as atoms, ions, and clusters, traveling with high kinetic energy. The species in the plume collide and react with molecules of the surrounding liquid, producing new compounds containing atoms from both the original target and the liquid. Because of the intensity of the laser and the nanosecond time scales, the instantaneous temperatures and pressure within the reaction volume can be extreme (many thousands of Kelvin at tens of giga-Pascals). Such high-temperature, high-pressure, and high-density conditions provide a "brute force" method of synthesizing novel materials that have hitherto been inaccessible using milder, more conventional techniques. Indeed, LP-PLA has proven to be an effective method for the preparation of many nanostructured materials, including nanocrystalline diamond,[18−20] cubic boron nitride,[21] and nanometer-sized particles of Ti,[22] Ag,[23] Au,[24] Zn,[25] and TiC.[26] However, to date, successful synthesis of crystallite carbon nitride by LP-PLA has not been reported in the literature.

Experimental Section

The experimental setup has been described in detail previously.[20] Briefly, a solid graphite target (Testbourne Ltd., 99.99%) was ablated at room temperature while submerged in a 5 ml solution of 35% (Fisher Scientific) ammonia solution inside a sealed stainless steel cell. The irradiation was supplied by the second harmonic of a Q-switched Nd:YAG laser (532 nm, pulse duration 15 ns) operating at 10 Hz with laser fluence from 25 to 125 mJ/pulse. The beam was directed by a prism and then focused using a 25 mm focal length lens through a quartz window in the top of the cell; the beam then went through a ~5 mm layer of the liquid covering the graphite, forming a ~0.5 mm diameter spot on the target surface. The cell was rotated at 700 rpm during ablation using a standard magnetic stirrer in order to reduce the effect of target aging. The ablation was typically carried out for periods up to 5 h, after which a colloidal suspension of nanoparticles remained in the container. The suspension changed from colorless to a pale brown as laser irradiation progressed, indicating an increase in solid product and/or a change in composition of the solid because of prolonged interaction with the laser. The suspension was stable, with no precipitate being observed if the sample tube remained untouched for up to two months.

For analysis by transmission electron microscopy (TEM), the suspension, containing a mixture of unreacted graphite and carbon nitride product(s), both in the form of nanoparticles, was pipetted onto a carbon-coated TEM grid, washed several times (using deionized water) to remove ammonia traces, and then allowed to dry to a powder in air. For analysis by X-ray photoelectron spectroscopy (XPS), the concentration of ablation products in the suspension needed to be increased by evaporation of some of the liquid phase in an oven. This concentrated suspension was then pipetted onto a glass slide and dried to produce a thin layer. This pipetting and drying procedure was repeated many times to increase the thickness of the layer until it was sufficient to obtain a high signal:noise ratio in the subsequent analysis.

Elemental analysis of the powder was performed using microcombustion, which gave quantitative values for the atomic percentage of C and N present. Powder X-ray diffraction (Bruker-AXS D8 powder diffractometer) was used to obtain information on bulk and microstructure composition. TEM and selected area electron diffraction (SAED) were used to identify the structure and morphology of the prepared materials. TEM was performed in bright-field mode using a JEOL 1200 EX electron microscope operating at 120 kV. High resolution (HR) TEM was carried on a JEOL 2010 electron microscope at 200 kV. X-ray photoelectron spectroscopy (XPS, Thermo VG Scientific) was used to search for evidence of C−N, C═C, and C≡N bonds, with Al-Kα (1486.6 eV) radiation operating at 400 W (15 kV). High-resolution scans were acquired with 30 eV pass energy and 200 ms dwell times.

Results and Discussion

General Structural Features. The elemental analysis (C, 38.56; N, 50.08; O, 9.31; H, 2.05 wt %) of the prepared product indicated that the average composition was $C_3N_{3.35}O_{0.54}H_{1.9}$, in comparison with the theoretical C_3N_4 empirical stoichiometry.[7,8] The presence of oxygen can be partly explained by the prolonged exposure of the samples to the laboratory atmosphere, leading to possible contamination by absorbed or adsorbed water vapor. Alternatively, the oxygen may be present as a result of reaction between the graphite surface and water (or OH radicals) as a result of the high temperatures in the plume.

The single broad peak in the X-ray diffraction pattern near 25.8° corresponds to an interlayer *d*-spacing of 3.42 Å, which is similar to the *d*-spacing reported for carbon nitride spheres[27,28] and in good agreement with the calculated values

(15) Matsumoto, S.; Xie, E. Q.; Izumi, F. *Diamond Relat. Mater.* **1999**, *8*, 1175.
(16) Muhl, S.; Méndez, J. M. *Diamond Relat. Mater.* **1999**, *8*, 1809.
(17) Yin, W. L.; Bando, Y.; Li, M. S.; Liu, Y. X.; Qi, Y. X. *Adv. Mater.* **2003**, *15*, 1840.
(18) Yang, G. W.; Wang. J. B. *Appl. Phys. A* **2001**, *72*, 475.
(19) Wang, J. B.; Zhang, C. Y.; Zhong, X. L.; Yang, G. W. *Chem. Phys. Lett.* **2002**, *361*, 86.
(20) Pearce, S. R. J.; Henley, S. J.; Claeyssens, F.; May, P. W.; Hallam, K. R.; Smith, J. A.; Rosser, K. N. *Diamond Relat. Mater.* **2004**, *13*, 661.
(21) Wang, J. B.; Yang, G. W.; Zhang, C. Y.; Zhong, X. L.; Ren, Z. H. A. *Chem. Phys. Lett.* **2003**, *367*, 10.
(22) Simakin, A. V.; Vornov, V. V.; Kirichenko, N. A.; Shafeev, G. A. *Appl. Phys. A* **2004**, *79*, 1127.
(23) Shafeev, G. A.; Freysz, E.; Bozon-Verduraz, F. *Appl. Phys. A* **2004**, *78*, 307.
(24) Sylvestre, J.-P.; Poulin, S.; Kasbashin, A. V.; Sacher, E.; Meunier, M.; Luong, J. H. T. *J. Phys. Chem. B* **2004**, *108*, 16864.
(25) Zeng, H.; Cai, W.; Li, Y.; Hu, J.; Liu, P. *J. Phys. Chem. B* **2004**, *109*, 18260.
(26) Dolgaev, S. I.; Simakin, A. V.; Voronov, V. V.; Shafeev, G. A.; Bozon-Verduraz, F. *Appl. Surf. Sci.* **2002**, *186*, 546.

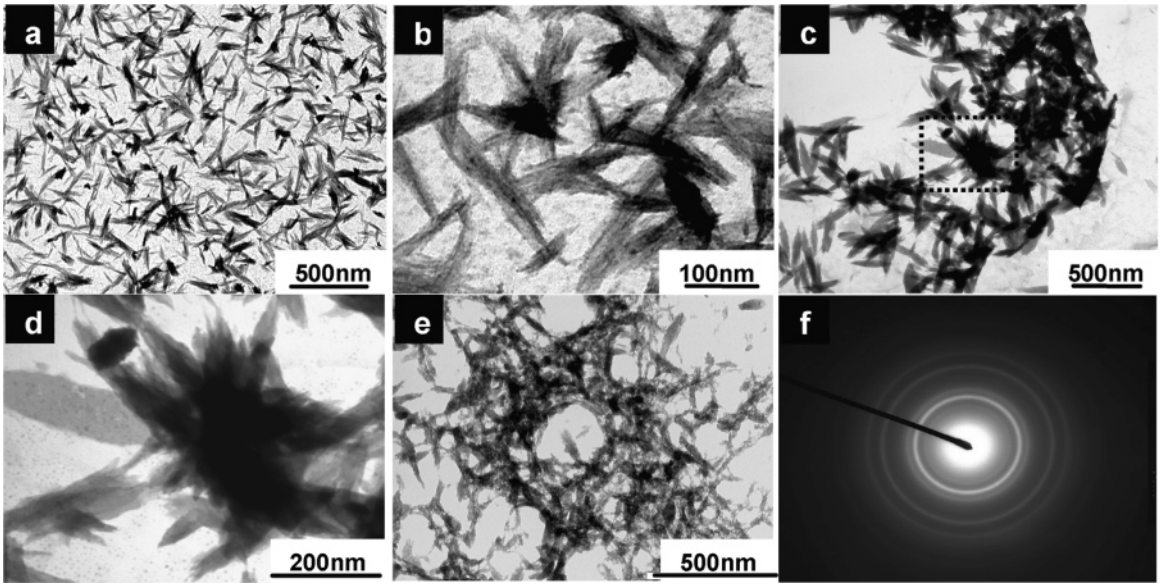

Figure 1. TEM images of samples produced by pulsed laser ablation of a graphite target in ammonia solution (laser fluence at 100 mJ per pulse) for durations of (a, b) 1, (c, d) 3, and (e) 5 h (laser power at 120 mJ). (a) Leaflike structures are formed after only short ablation times. The higher magnification image of these, image (b), shows that these structures are composed of smaller nanorods. For longer ablation times, image (c), the leaflike structures increase in size and coalesce to form larger, denser, structures. The higher-magnification image (d) of the region enclosed by the dashed lines shows that the surface of these structures is smooth. For even longer ablation times, image (e), the denser structures begin to assemble together to form microscale networks. (f) A typical SAED pattern from the leaflike nanostructures in image (a), which corresponds closely to the calculated interlayer *d*-spacing of β-C_3N_4.

for α-C_3N_4 and β-C_3N_4 in the hexagonal lattice reported in refs 29 and 30.

The TEM analysis revealed that the ablated product contained a mixture of amorphous carbon and graphite from the target, plus a range of unusual carbon nitride nanostructures depending upon the process conditions and especially upon ablation time. These nanostructures were most likely formed as a result of the self-organizing and close packing of the nanoparticles as the suspension was dried out. Figure 1a,b shows that after 1 h of ablation (laser fluence at 100 mJ per pulse), one-dimensional structures are formed that are ~200 nm in length and 30−50 nm in width. Because both ends of the flat structures taper to a point, they resemble the shape of a leaf, and so henceforth have been termed leaflike structures. The high-magnification image (Figure 1b) shows that these structures are themselves composed of a large number of smaller nanorods that have packed together in an ordered arrangement to form the leaflike shapes. After ablation times of ~3 h (Figure 1c,d), the leaflike structures coalesce to form larger, denser structures with a smooth surface, which start to connect together. For ablation times around 5 h and laser power at 125 mJ (Figure 1e), these denser structures form a network of microscale structures.

Figure 1f shows a typical SAED ring pattern (obtained without any tilting) from the leaflike nanostructures in Figure 1a, which indicates that these structures are polycrystalline. The four inner rings, with interlayer *d*-spacings of 3.176, 2.727, 1.938, and 1.630 Å, respectively, were indexed as (110), (200), (111), and (220) with reference to the calculated structure for β-C_3N_4.[6,8,30−31] On the basis of the assumption of a hexagonal structure, we calculated the lattice indices of a_0 and c_0 to be 6.3520 and 2.446 Å from the spacing of the (110) and (111) planes, which are both slightly lower than the theoretical values reported previously (a = 6.4017 Å, c = 2.4041 Å, space group: $P6_3/m$ (No. 176)).[8,30] These results are consistent with the SAED patterns and peaks previously assigned to single-crystalline carbon nitride nanorods.[17]

Chemical-Bonding Environment. The XPS spectrum of the ablation product shows peaks for carbon and nitrogen as expected, but also for oxygen, other surface impurities and adsorbates. The C 1s peak (Figure 2a) has been deconvoluted into two peaks centered at 284.8 and 287.7 eV. The peak at 284.8 eV has been assigned previously as graphitic carbon, which includes contributions from graphite-like or amorphous carbon within the material along with adventitious carbon adsorbed on the surface (284.6 eV), as well as C═C (284.6 eV), sp^3 C−C (284.7 eV), and C═N (284.8 eV).[12,32−34] However, the peak at 287.7 eV has been assigned only to sp^3-bonded C in C−N,[35] with some workers[32−34] also assigning the highest deconvoluted peak to sp^3 C−N but at a slightly lower energy (~287.0 eV). The XPS study of CN_x films by Le Normand et al.[36] further states that the presence of sp^3 C−N is indicated by the presence of all peaks between 287.2 and 287.7 eV. Therefore, it can be concluded that sp^3 C−N bonds are present in the ablated product, which is consistent with C_3N_4. The N 1s feature

(27) Liu, A. Y.; Cohen, M. L. *Phys. Rev. B* **1990**, *41*, 10727.
(28) Wang, J.; Lei, J.; Wang, R. *Phys. Rev. B* **1998**, *58*, 11890.
(29) Vinu, A.; Ariga, K.; Mori, T.; Nakanishi, T.; Hishita, S.; Golberg, D.; Bando, Y. *Adv. Mater.* **2005**, *17*, 1648.
(30) Zimmerman, J. L.; Williams, R.; Khabashesku, V. N.; Margrave, J. L. *Nano Lett.* **2001**, *1*, 731.
(31) Guo, Y.; Goddard, W. A., III. *Chem. Phys. Lett.* **1995**, *237*, 72.
(32) Boyd, K.; Marton, D.; Todorov, S. S.; Al Bayati, A. H.; Kulik, J.; Zhur, R. A.; Rabalais, J. W. *J. Vac. Sci. Technol., A* **1995**, *13*, 2110.
(33) Tabbal, M.; Merel, P.; Moisa, S.; Chaker, M.; Ricard, A.; Moisan, M. *Appl. Phys. Lett.* **1996**, *69*, 1698.
(34) Angleraud, B.; Mubumbila, N.; Tessier, P. Y.; Fernandez, V.; Turban, G. *Diamond Relat. Mater.* **2001**, *10*, 1142.
(35) Shi, J. R.; Xu, Y. J.; Zhang, J. *Thin Solid Films* **2005**, *483*, 169.
(36) Le Normand, F.; Hommet, J.; Szorenyi, T.; Fuchs, C.; Fogarassy, E. *Phys. Rev. B* **2001**, *64*, 235416.

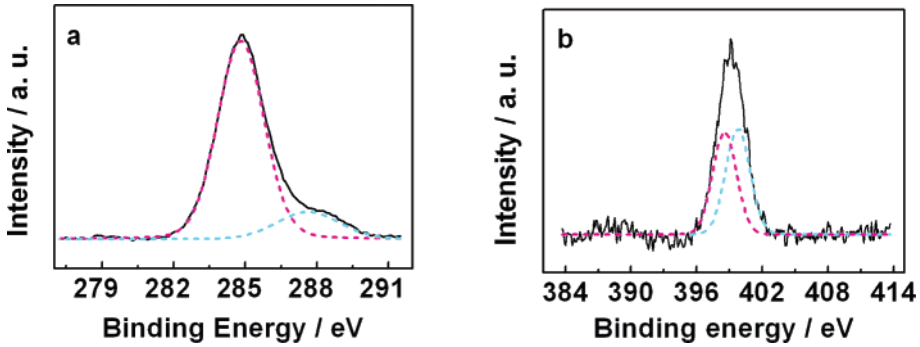

Figure 2. (a) C 1s and (b) N 1s XPS spectra of the product obtained from LP-PLA after 5 h of ablation. After background subtraction, the spectra were deconvoluted into two Gaussian line-shaped peaks centered at 284.8 and 287.7 eV in (a) and 398.8 and 400.0 eV in (b).

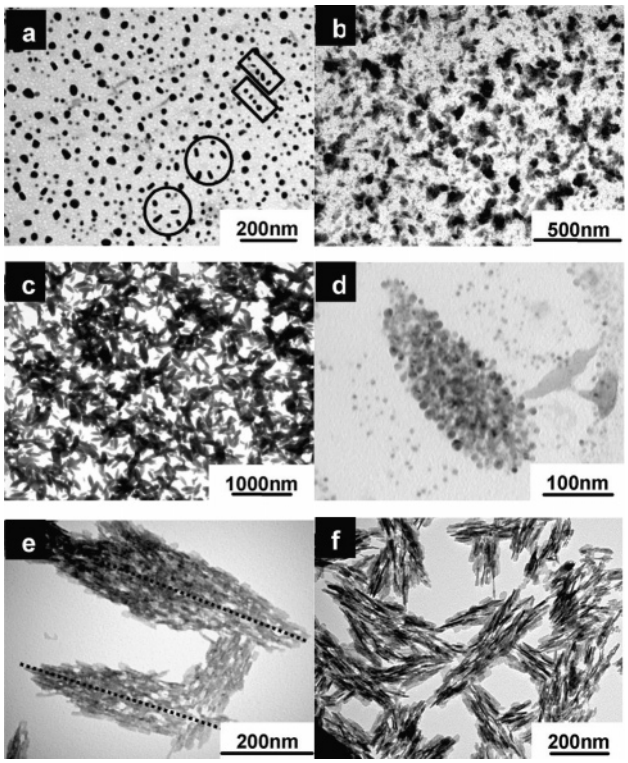

Figure 3. TEM images of C_3N_4 nanostructures synthesized at 75 mJ/pulse laser fluence for different ablation times. (a) After 10 min ablation, spherical nanoparticles appear, with an average particle size of 15−20 nm. Adjacent particles are aligned with one another along their main axes, highlighted by the inset rectangles. Short rods (highlighted by circles) have already formed and serve as the starting structures for the subsequent formation of leaflike structures. (b) After 30 min ablation, there is a mixture of leaf-shaped structures and their component nanoparticles. (c) After 3 h ablation, the leaflike structures are larger, better developed, and have a smooth surface. (d) Single "leaf" formed by numerous small nanoparticles. (e) Interconnected leaflike structures formed by nanorods. Note that those rods perpendicular to the propagating axis (*c*-axis, dashed line in the picture) along the structure were well-aligned. (f) High-magnification image showing that after 5 h ablation time, the nanorods inside the leaflike structures have not changed in size or shape.

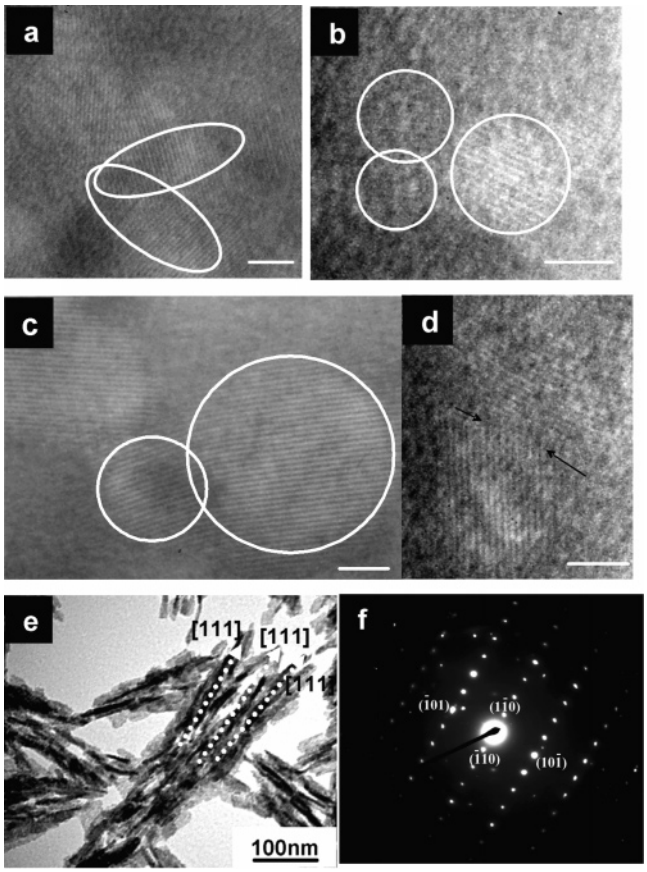

Figure 4. (a−d) HRTEM images of a series of aggregated particles; scale bar is 2 nm. (a) Interconnection of two leaflike structures is highlighted by the two ringed areas. (b) Size of the internal nanoparticles is about 3−5 nm. (c) Lattice planes go straight through the interface between the particles, which means the particles are fused together with no interlayer separating them. (d) High-magnification image of a grain boundary, shown by the arrows. (e) Nanorod aggregates exhibit a long-range order; arrows indicate the projecting direction along [111]. (f) SAED pattern of a nanorod from the [111] zone axis indicating the area is single crystal and consistent with crystalline β-carbon nitride.

(Figure 2b) is more difficult to assign unambiguously, because it is known that N can give broad XPS peaks in some materials. Thus, the feature around 399 eV could be one broad peak from N in a single-bonding configuration. Alternatively, the feature can be deconvoluted into two peaks (as shown in Figure 2b), one at 398.8 eV assigned to sp^3 C−N bonds, and one at 400.0 eV assigned to sp^2 C═N bonds.[9,32−36] However, within experimental accuracy, it is impossible to distinguish between these two alternatives. Also, it should be noted that C≡N bonds can also produce three peaks in this region, at 398.2,[37] 398.1,[38] and 400.1 eV.[39] However, these assignments have been discounted, because they are outside the experimental accuracy of the XPS

(37) Ripalda, J. M.; Montero, I.; Galan, L. *Diamond Relat. Mater*. **1998**, *7*, 402.
(38) Ogata, K.; Chubaci, J. F. D.; Fujimoto, F. *J. Appl. Phys*. **1994**, *76*, 3791.
(39) Khabashesku, J. V. N.; Zimmerman, L.; Margrave, J. L. *Chem. Mater*. **2000**, *12*, 3264.

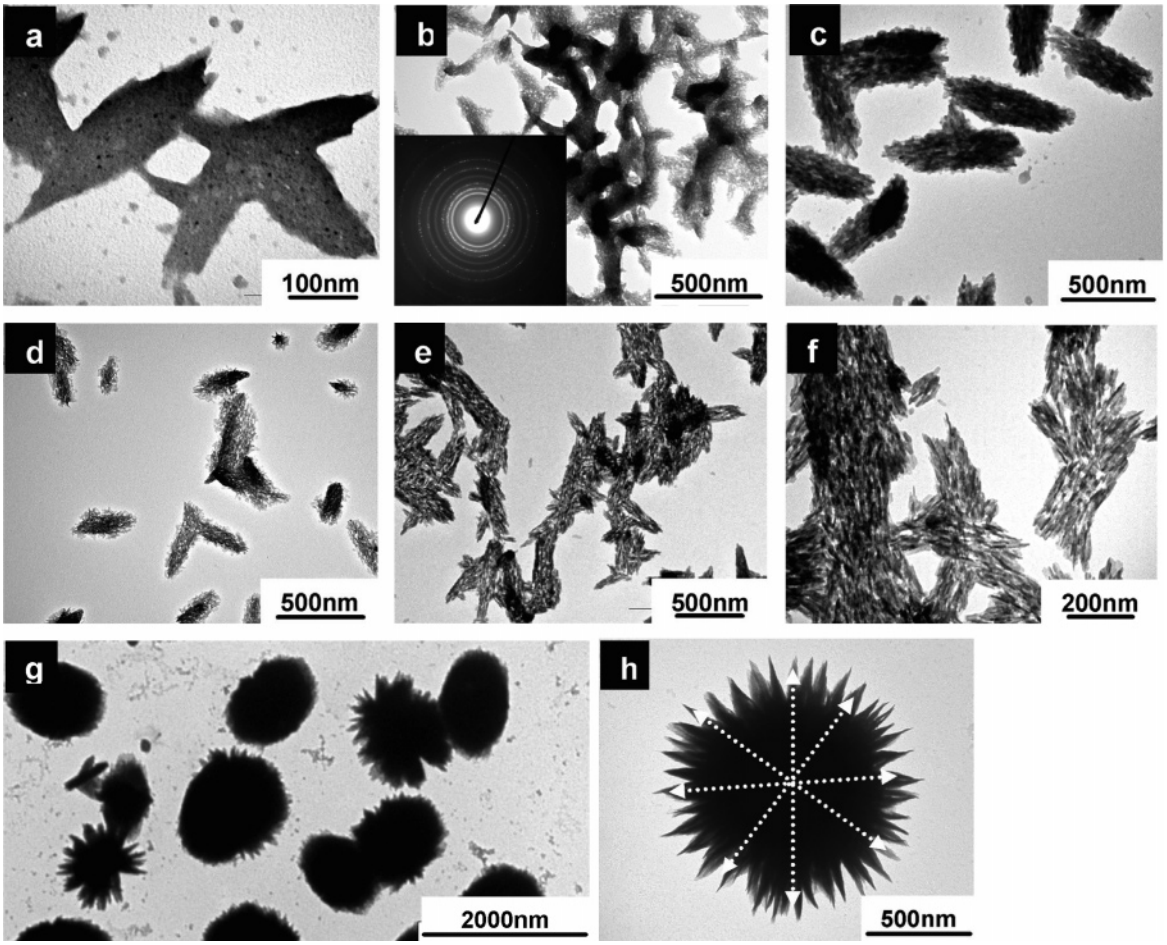

Figure 5. TEM images of C_3N_4 nanostructures synthesized for 3 h ablation time using different laser fluences: (a, b) 25 mJ/pulse, leaflike structures containing spherical nanoparticles and short nanorods. Inset in (b) is a sharp SAED pattern, indicating the structures are crystalline. Note that there appear to be voids inside the leaflike structures (the white areas in the gray area of image (b)); (c, d) 50 mJ/pulse, denser leaflike structures containing longer nanorods that protrude from the surface. (e, f) 75 mJ/pulse, leaflike structures beginning to aggregate into larger clumps. (g, h) 100 mJ/pulse, carbon nitride nanospheres and flowerlike spiky crystallites.

spectrometer. The presence of sp^3 C−N in the ablated nanostructures is, again, in agreement with a C_3N_4 structure.

Varying Ablation Time. To understand the formation mechanism of nanocrystalline carbon nitride, we performed experiments for different ablation times with the laser fluence constant at 75 mJ/pulse. Figure 3a shows that spherical particles appeared after only 10 min ablation. The areas highlighted by circles and rectangles in Figure 3a indicate that some of the particles may be lining up, which suggests that they might subsequently coalesce into a nanorod. Alternatively, nanorods may form by one-dimensional nanoparticle growth, as nanoparticles add preferentially to the ends of a line of nanoparticles. Whichever mechanism is correct, it is clear that nanorod formation, growth, and aggregation all occur on a short time scale.

With longer ablation times, the nanorods start to aggregate into multilayered structures, serving as the starting points (or nucleation seeds) for the subsequent growth. After ∼30 min ablation time, we observe (Figure 3b) a mixture of different sized nanoparticles, along with some that have begun to coalesce into leaflike shapes. As ablation continues, these leaflike structures increase in size, as can be seen in Figure 3c. Figure 3d,e shows that these leaflike nanostructures are mostly made of component nanoparticles or nanorods. With even longer ablation times (5 h), the length and width of the internal nanorods (width ∼5−10 nm, length ∼30−100 nm) remained almost constant (Figure 3f), but the number of leaflike structures increased with all the well-aligned internal nanorods pointing in the same direction, perpendicular to the propagating *c*-axis (Figure 3e,f).

High-resolution TEM images of a series of aggregated particles are shown in Figure 4. It is seen that the lattice planes of the particles are almost perfectly aligned. Some leaflike structures are interconnected (Figure 4a), and the lattice planes of each particle are fused directly, with no evidence for an amorphous boundary interlayer (Figure 4b−d). Although individual leaflike structures within a local region seem to be randomly oriented, the overall nanorod aggregates still exhibit long-range ordering[40,41] (Figure 4e). A representative SAED pattern is given in Figure 4f, showing diffraction spots from the $(\bar{1}10)$, $(1\bar{1}0)$, $(\bar{1}01)$, and $(10\bar{1})$ planes of the [111] zone axis, which are aligned parallel each other. Therefore, a clear crystallographic relationship exists among the [111]-oriented crystallites.[42] Indeed, in Figure 7a−d, most of the observed lattice planes in these images are the (111) plane corresponding to crystalline β-carbon nitride

(40) Pacholski, C.; Kornowski, A.; Weller, H. *Angew. Chem., Int. Ed.* **2002**, *41*, 1188.
(41) Zeng, H. C. *J. Mater. Chem.* **2006**, *16*, 649.
(42) Liu, B.; Zeng, H. C. *Small* **2005**, *1*, 566.

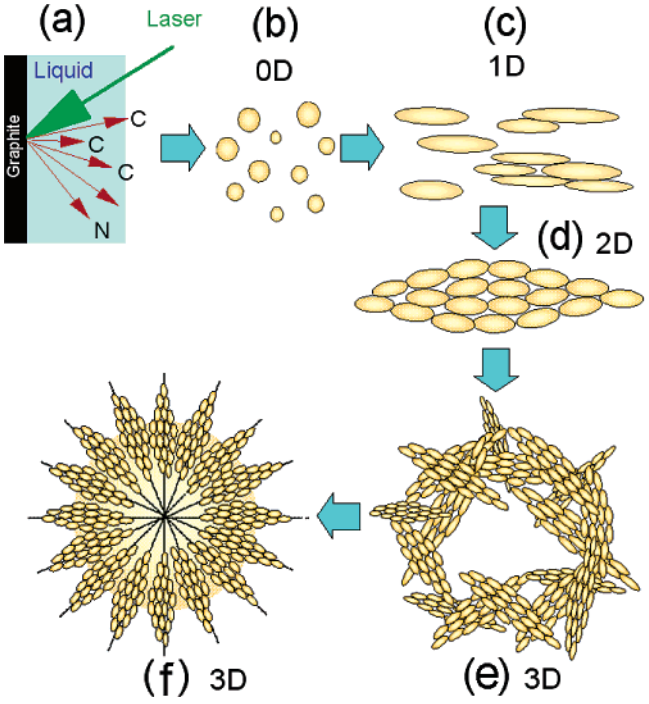

Figure 6. Proposed sequential growth pathway model involving structural and morphology modifications of carbon nitride, with increasing ablation time (and concentration). (a) The ablation plume creates energetic C and N species. (b) The species condense into monodispersed spherical C_3N_4 one-dimensional nanoparticles. (c) Nanoparticles elongate into two-dimensional rods, and these start to aggregate to form multilayer structures. (d) The multilayered structures increase in size until they form leaflike structures 40 nm by ~200 nm in size. (e) The leaflike structures aggregate into a network of three-dimensional joined clusters. (f) Clusters undergo a phase transformation to produce micrometer scale flowerlike particles with multifold symmetry.

with an interplanar distance of 0.193 nm,[31] and they lie perpendicular or parallel to the *c*-axis.

Varying Laser Fluence. Figure 5 shows TEM images of C_3N_4 nanostructures synthesized for 3 h ablation time with varying laser fluences. For low laser fluence (25 mJ/pulse), the leaflike structures had a length and width of ~300 and ~120 nm, respectively, smooth surfaces, and were composed of smaller-sized nanorods (Figure 5a). There were also plenty of voids situated between some of the nanorods (Figure 5b). The sharp SAED pattern for the leaflike structures (inset Figure 5b) was consistent with crystalline hexagonal β-phase carbon nitride.[30,31] When the laser power was increased to 50 mJ/pulse, the aligned leaf-like structures increased to a length and width of ~600 and ~250 nm, respectively (Figure 5c,d) and now consisted of a substantial number of connected nanorods, although there was no apparent change in size of the component nanorods. The surface of the leaflike structure was no longer smooth, but contained numerous protruding nanorods. For still-higher fluences (75 mJ/pulse), there was no further significant change in the size or shape of the leaflike structures and nanorod building units (Figure 5e,f), but there was an increase the number formed. With further increases in fluence to 100 mJ/pulse, micrometer-scale carbon nitride spheres (Figure 5g) were observed, formed by aggregation of a large number of the leaflike structures. Flowerlike spiked crystallites (Figure 5h) were also seen, where the leaflike structures coalesced at a common center with multifold symmetry.[43] In particular, the trend is that the size of the overall nanocrystallites and their basic building blocks increases with increasing laser power.

Proposed Mechanism of Formation. In light of these results, a model for the sequential growth pathway has been proposed, illustrated in Figure 6, involving structural and morphology modifications of carbon nitride. This complicated reaction process could generally be expressed in terms of following overall equation: $4NH_3 + 3C \rightarrow C_3N_4 + 6H_2$. This is consistent with the chemical mechanism proposed in a recent study by Yin et al.[17] The highly energetic C and N species in the ablation plume (Figure 6a) initially condense into small monodispersed spherical C_3N_4 nanoparticles (Figure 6b). Because of the very short laser pulse length (15 ns) and the fact that the plume is rapidly quenched by the surrounding liquid, the growth times of these nuclei are very short. This may aid the preferential formation of small metastable nuclei with a uniform particle distribution,[44] as seen in Figure 3a. With increasing concentration (caused by longer ablation times), the spherical C_3N_4 nuclei begin to join together to form short rods (Figure 6c),[45] which then elongate on exposure to more laser energy as a result of chemical reactions with the liquid phase.[46] When the concentration of the nanorods becomes sufficiently high, they begin to line up to form multilayer leaflike structures (Figure 6d). With increasing density of leaflike structures in the suspension, the leaflike structures themselves begin to aggregate into large connected networks (Figure 6e), which eventually rearrange to form mesoscale superstructures, such as spheres and finally flowerlike structures (Figure 6f).

Conclusions

In this one-step synthesis, a liquid−solid mechanism has been described that uses simple, room-temperature, solution−solid-phase reactions for the growth of C_3N_4 by pulsed laser ablation. Evidence has been provided to illustrate that the various nanostructured materials produced in this way are composed of crystalline α- or β-C_3N_4. The morphology of the crystalline material changes at different length scales. The basic building blocks are nanoparticles/nanorods (10 nm by ~200 nm), which, given sufficient concentration, then aggregate to form larger, ordered leaflike structures (30−50 nm by ~200 nm). Other geometrically complex C_3N_4 nanostructures, such as interconnected networks, large mesoscale clusters, and multifold-symmetry flowerlike structures, can also be fabricated via a self-assembly ordered scheme.

Further evidence for these findings may be obtained by using a technique such as electron energy loss spectroscopy (EELS), which would be able to distinguish between N bonded to C (as in C_3N_4) or as some other form. Future studies may also include the use of other nitrogen-containing liquids (such as hydrazine), which may facilitate the generation of nitrogen atoms and radicals more readily. Addition of surfactants into the solution may also influence the aggregation and dispersal of the nanomaterials. Similar synthesis

(43) Liu, B.; Zeng, H. C. *J. Am. Chem. Soc.* **2004**, *126*, 16744.
(44) Yang, G. W.; Wang, J. B. *Appl. Phys. A* **2000**, *71*, 343.
(45) Liu, B.; Zeng, H. C. *J. Am. Chem. Soc.* **2004**, *126*, 8124.
(46) Shaw, S. J.; Schiffers, W. P.; Gentry, T. P.; Emmony, D. C. *J. Phys. D: Appl. Phys.* **1999**, *32*, 1612.

routes for other Group IV−V crystalline compounds may also be possible using this "brute force" LP-PLA approach, and appropriate target materials and liquids will be explored.

Acknowledgment. We thank Dr. S. A. Davis, J. Jones, K. N. Rosser, C. Archer, and Dr. J. Smith for their many and varied contributions to the work described herein. This research has been supported by Universities UK via Overseas Research Scholarship (ORS) and by the University of Bristol and its School of Chemistry.

CM061485E